







The fates of internalized Na_v1.7 channels in sensory neurons: Retrograde cotransport with other ion channels, axon-specific recycling, and degradation

Received for publication, May 16, 2022, and in revised form, December 5, 2022. Published, Papers in Press, December 17, 2022.

<https://doi.org/10.1016/j.jbc.2022.102816>

Grant P. Higerd-Rusli^{1,2,3,4} , Sidharth Tyagi^{1,2,3,4}, Shujun Liu^{2,3,4}, Fadia B. Dib-Hajj^{2,3,4} ,
Stephen G. Waxman^{2,3,4,*} , and Sulayman D. Dib-Hajj^{2,3,4,*} 

From the ¹MD/PhD Program, Yale University School of Medicine, New Haven, Connecticut, USA; ²Center for Neuroscience and Regeneration Research, Yale University School of Medicine, New Haven, Connecticut, USA; ³Department of Neurology, Yale University School of Medicine, New Haven, Connecticut, USA; ⁴Rehabilitation Research Center, Veterans Affairs Connecticut Healthcare System, West Haven, Connecticut, USA

Edited by Phyllis Hanson

Neuronal function relies on the maintenance of appropriate levels of various ion channels at the cell membrane, which is accomplished by balancing secretory, degradative, and recycling pathways. Neuronal function further depends on membrane specialization through polarized distribution of specific proteins to distinct neuronal compartments such as axons. Voltage-gated sodium channel Na_v1.7, a threshold channel for firing action potentials in nociceptors, plays a major role in human pain, and its abundance in the plasma membrane is tightly regulated. We have recently characterized the anterograde axonal trafficking of Na_v1.7 channels in Rab6A-positive vesicles, but the fate of internalized channels is not known. Membrane proteins that have undergone endocytosis can be directed into multiple pathways including those for degradation, recycling to the membrane, and transcytosis. Here, we demonstrate Na_v1.7 endocytosis and dynein-dependent retrograde trafficking in Rab7-containing late endosomes together with other axonal membrane proteins using real-time imaging of live neurons. We show that some internalized Na_v1.7 channels are delivered to lysosomes within the cell body, and that there is no evidence for Na_v1.7 transcytosis. In addition, we show that Na_v1.7 is recycled specifically to the axonal membrane as opposed to the soma membrane, suggesting a novel mechanism for the development of neuronal polarity. Together, these results shed light on the mechanisms by which neurons maintain excitable membranes and may inform efforts to target ion channel trafficking for the treatment of disorders of excitability.

Sensory neurons within the dorsal root ganglion (DRG) rely on the function of several voltage-gated sodium (Na_v) channels to generate action potentials (1). Na_v channel activity underpins the function of nearly all excitable tissues (including the brain, heart, and muscle), and individual Na_v isoforms are expressed in a tissue-dependent manner (2). Na_v1.7 is

expressed preferentially in peripheral neurons, including nociceptors (3, 4). Na_v1.7 plays a major role in the physiology of pain because it sets the activation threshold for nociceptors (pain-sensing neurons) (5–9). Furthermore, genetic studies show that Na_v1.7 is an obligate mediator of pain sensation in humans, causing both syndromes of extreme pain when mutations increase its activity and congenital insensitivity to pain when its function is impaired (10, 11). Together, these factors have made selective blockade of Na_v1.7 function a promising target for nonaddictive analgesia (12, 13).

Neuronal excitability is shaped by the activity and number of ion channels in the cell membrane, which depends on the balancing of channel production, subcellular distribution, exocytosis, endocytosis, recycling, and degradation (14). Since the function of ion channels is dependent on their presence at the cell membrane, dysfunction of channel trafficking is predicted to underlie excitability disorders. Thus, modulating their trafficking could potentially be used as a therapeutic strategy to treat these disorders including pain. Our understanding of these processes for full-length Na_v channels is currently limited because studying them was until recently not possible, especially at axonal ends far from the soma. We have now developed methods that have enabled real-time visualization of anterograde trafficking and surface distribution of single Na_v channels in sensory axons (15). However, the fates of Na_v channels after they undergo endocytosis remain unexplored and potentially include degradation, recycling back to the membrane, and the circuitous pathway of transcytosis, whereby proteins are first inserted in a somatodendritic compartment, internalized, and finally trafficked anterogradely to the axon (16). Furthermore, endosomes originating in distal axons undergo a maturation process as they are trafficked retrogradely to the cell body, which includes conversion from a state of association with Rab5 to association with Rab7 (small GTPases linked with early and late endosomes, respectively) and eventual delivery to the lysosome (17). The state of maturity of endosomes carrying Na_v1.7 in axons is not known.

Neurons are among the most morphologically complex cells, and their function depends on localization of specific

* For correspondence: Sulayman D. Dib-Hajj, sulayman.dib-hajj@yale.edu; Stephen G. Waxman, stephen.waxman@yale.edu.

The fates of internalized Na_v channels in sensory neurons

membrane proteins in specialized domains such as neurotransmitter receptors in postsynaptic terminals and Na_v channels in the axon initial segment (AIS) and nodes of Ranvier in myelinated axons (18). Neurons utilize a variety of mechanisms to establish and maintain this polarization, including directly trafficking and trapping of specific Na_v channel isoforms within the AIS in an ankyrin G–dependent manner, and possible selective endocytosis from the somato-dendritic membrane in hippocampal neurons (19, 20). However, unmyelinated axons are not known to possess similar well-delineated axonal membrane specializations, and the regulation of the distribution of Na_v channels in these neurons is less well understood.

We report here the first observations of the fates of internalized full-length $\text{Na}_v1.7$ channel in unmyelinated axons, including retrograde transport, domain-specific recycling, and degradation. Using cell-impermeable fluorescent ligands and compartmentalized neuronal cultures in microfluidic chambers (MFCs) together with super-resolution microscopy, we demonstrate ongoing endocytosis and retrograde trafficking of $\text{Na}_v1.7$ in distal axons, which is dynein dependent. Furthermore, we demonstrate that some internalized $\text{Na}_v1.7$ channels

are transported retrogradely in Rab7 late endosomes, together with multiple other axonal membrane proteins before delivery to lysosomes in cell bodies, whereas there was no evidence for $\text{Na}_v1.7$ transcytosis. We have also observed specific recycling of internalized $\text{Na}_v1.7$ channels in axonal membrane but not soma. These studies fill fundamental knowledge gaps regarding the fate of internalized Na_v channels and uncover an additional mechanism for maintenance of polarized distribution of axonal proteins, which may inform efforts to target ion channel trafficking for the treatment of disorders of excitability.

Results

$\text{Na}_v1.7$ undergoes endocytosis and retrograde trafficking in distal axons

We previously engineered an $\text{Na}_v1.7$ channel with an N-terminal Halo tag, a self-labeling enzyme that covalently reacts with specific photostable synthetic ligands, along with an additional transmembrane domain resulting in an extracellularly tagged channel with 25 transmembrane segments (Fig. 1A) (15). To study the trafficking of these channels in

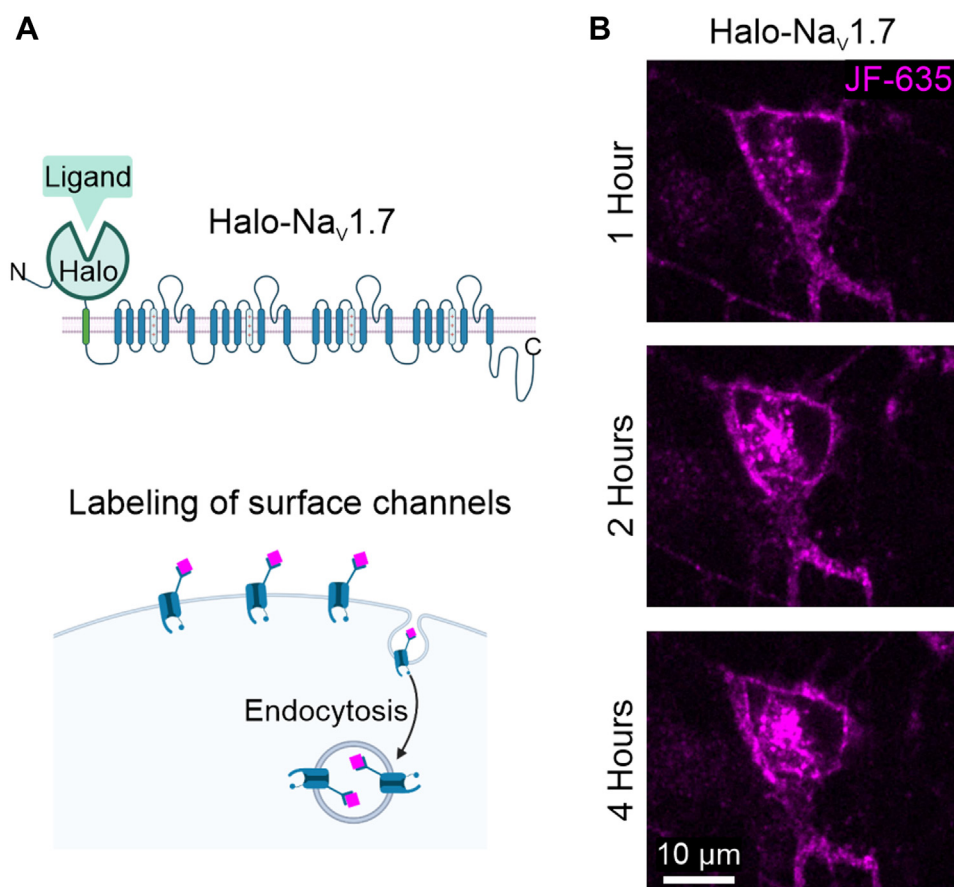


Figure 1. Surface-labeled $\text{Na}_v1.7$ channels undergo endocytosis. A, the Halo- $\text{Na}_v1.7$ channel features the Halo-tag enzyme fused to the extracellular N terminus of the channel via an extra transmembrane segment (top panel). DRG neurons were transfected with Halo- $\text{Na}_v1.7$ and cultured for 5 days. Cell-impermeable Halo-tag ligand covalently labels channels that are at the cell surface and subsequently undergo endocytosis (bottom panel). B, $\text{Na}_v1.7$ channels initially at the cell surface are translocated into the cytoplasm. DRG neurons transfected, cultured, and labeled with Halo-tag ligand JF635i as described in (A) were imaged by spinning-disc confocal microscopy in a stage-top incubator at 37 °C for several hours. While fluorescence was initially restricted to the perimeter of transfected cells, over time, more signal was seen within the cytoplasm. DRG, dorsal root ganglion; Na_v , voltage-gated sodium channel.

The fates of internalized Na_v channels in sensory neurons

distal axons, we transfected the channel construct into DRG neurons. Also, we utilized MFCs to create compartmentalized cultures where DRG somata are isolated from their axons (Fig. 2A). We first visualized the endocytosis of $\text{Na}_v1.7$ channels from the soma membrane by adding fluorescent and cell-impermeable Halo-tag ligands (21) to the soma chamber to label only channels at the cell surface, which can then be observed as they are internalized and trafficked within the cell. Indeed, 1 h after labeling with Halo-tag JF635i (where “i” denotes cell impermeability), DRG cell bodies expressing Halo- $\text{Na}_v1.7$ channels showed fluorescence limited to the cell membrane. However, over time, more fluorescence signal appeared within the cytoplasm (Fig. 1B), whereas signal disappeared from parts of the soma membrane. During all live-cell time-lapse imaging, cells were kept in a stage-top incubator at 37 °C.

When Halo-tag ligand JF635i was applied to distal axons, fluorescence was initially distributed diffusely along the axon. However, within a matter of minutes, fluorescent puncta began to appear in the distal axon. These puncta were initially stationary, but some eventually began moving in the retrograde

direction (Fig. 2B). Based on their retrograde movement and colocalization with endosomal markers (Fig. 3), we refer to these moving puncta as endosomes henceforth. When axons were observed over longer periods of up to an hour, many endosomes were seen moving retrogradely (Fig. 2C). Furthermore, in axons treated with the dynein inhibitor ciliobrevin D, $\text{Na}_v1.7$ puncta formed in distal axons but were not trafficked retrogradely. These stationary puncta likely reflect endosomes that are arrested in the distal axon. The instantaneous velocity (excluding long pauses) of moving $\text{Na}_v1.7$ endosomes that had begun moving in untreated axons was distributed around a mean of 0.52 $\mu\text{m}/\text{s}$ in the retrograde direction, with very few endosomes moving anterogradely (Fig. 2D). The velocity of these endosomes was comparable with previous measurements of dynein-dependent trafficking (22–24). The number of endosomes being transported retrogradely varied with time after labeling, with fewer being seen in the first 20 min of imaging (corresponding to the period 30–50 min after the start of labeling) after which the rate reached a plateau (Fig. 2E). This suggests that there is a minimum period required for Na_v channels to undergo

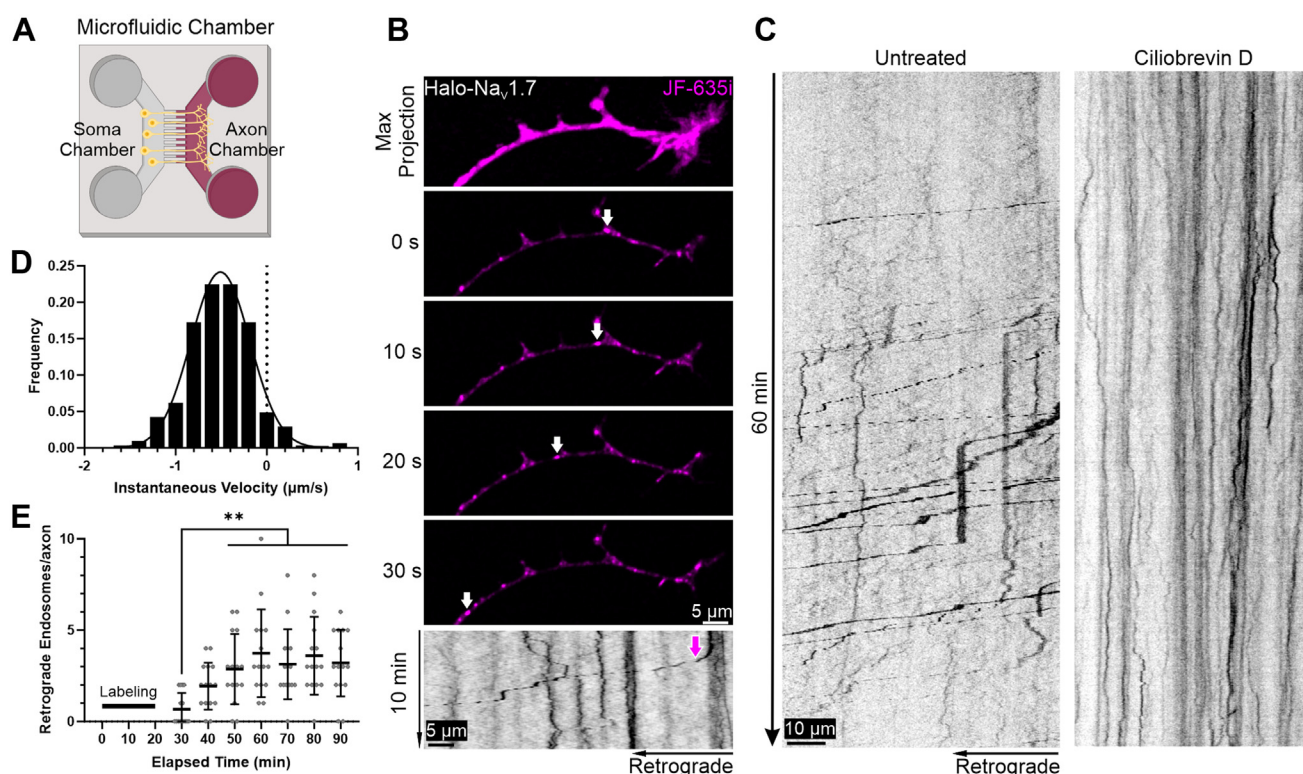


Figure 2. $\text{Na}_v1.7$ channels undergo endocytosis and dynein-dependent retrograde trafficking in distal axons. A, DRG neurons were transfected with Halo- $\text{Na}_v1.7$ and cultured in microfluidic chambers (MFCs) for 5 days, allowing axons to grow into the distal axon chamber. Channels at the surface of distal axons were labeled with cell-impermeable Halo-tag ligand JF635i. B, $\text{Na}_v1.7$ channels labeled at the surface of distal axons formed bright puncta, some of which were trafficked retrogradely, which we will refer to as endosomes. The top panel shows a maximum intensity projection of a 10 min movie of a distal axon, illustrating the axon's outline. The middle panels are still images from the movie above, in which a fluorescent signal begins moving in the retrograde direction (white arrows). The bottom panel is a kymograph plot of the above axon, which displays distance along the axon as the x-axis and elapsed time on the y-axis. Stationary fluorescence puncta appear as vertical lines, whereas a retrogradely moving particle moves from the upper right to lower left (magenta arrow). C, a kymograph from a 1 h time-lapse movie of an untreated axon shows that endosomes containing surface-labeled $\text{Na}_v1.7$ moved along axons almost exclusively in the retrograde direction. $\text{Na}_v1.7$ in axons treated with ciliobrevin D (20 μM) form puncta, which remain arrested in the distal axon. D, the instantaneous velocity of $\text{Na}_v1.7$ -containing endosomes that had begun moving was distributed around a mean of 0.52 $\mu\text{m}/\text{s}$ in the retrograde (negative) direction. E, the number of endosomes being trafficked retrogradely varied with time after the start of labeling, with fewer seen in the first 20 min of imaging (30–50 min after the start of labeling) and reached a plateau 50 min after the start of labeling ($p < 0.01$, Kruskal–Wallis test with Dunn's correction, $N = 307$ endosomes from 15 axons and 2 cultures). Error bars indicate mean \pm SD). DRG, dorsal root ganglion; Na_v , voltage-gated sodium channel.

The fates of internalized $\text{Na}_v1.7$ channels in sensory neurons

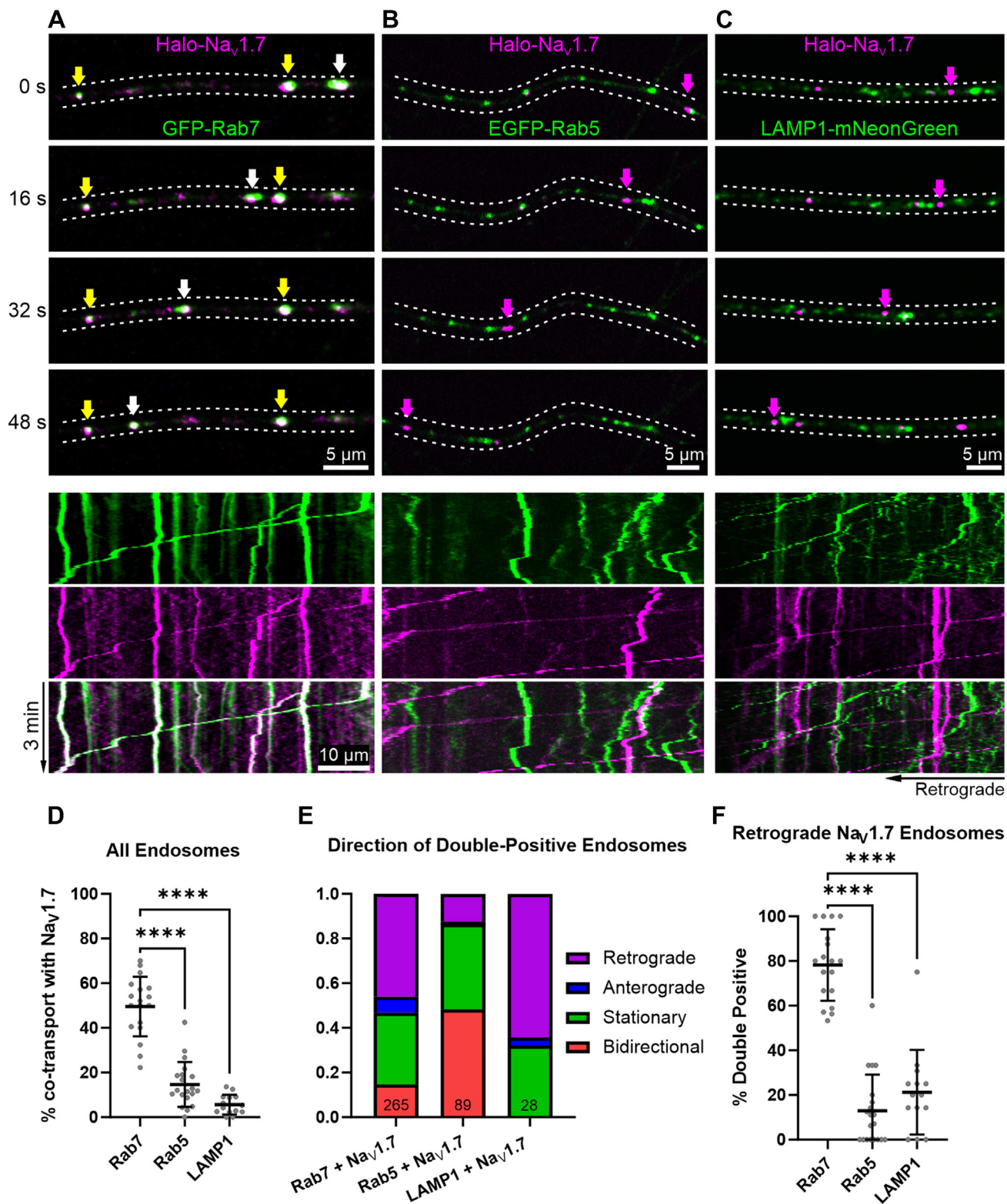


Figure 3. Internalized $\text{Na}_v1.7$ channels are transported retrogradely in Rab7 endosomes. DRG neurons were transfected with Halo- $\text{Na}_v1.7$ and either GFP-Rab7, EGFP-Rab5, or LAMP1-mNeonGreen (markers of late endosomes/multivesicular bodies, early endosomes, or lysosomes, respectively) and cultured in MFCs for 5 days. $\text{Na}_v1.7$ at the surface of distal axons were labeled using cell-impermeable Halo-tag ligand JF635i, and videos of axons were recorded in both green and far-red (JF635i) channels. Since few retrogradely moving endosomes are visible in the first 30 min after the start of surface labeling, axons were imaged 40 to 90 min after the start of labeling. *A*, upper panels show still images of a distal axon expressing both Halo- $\text{Na}_v1.7$ and GFP-Rab7 including multiple endosomes that contain both markers: two of which are stationary (yellow arrows) and one of which is moving in the retrograde direction (white arrow). Lower panels display a kymograph generated from the above axon demonstrating colocalization over time and space. *B* and *C*, upper panels show still images of a distal axon expressing Halo- $\text{Na}_v1.7$ and EGFP-Rab5 (*B*) or LAMP1-mNeonGreen (*C*). $\text{Na}_v1.7$ endosomes (magenta arrows) moved in the retrograde direction independently of Rab5 and LAMP1 vesicles. Lower panels display kymographs from the above axons. *D*, the rate of cotransport (the fraction of all observed vesicles that were double positive) for Halo- $\text{Na}_v1.7$ and Rab7 was greater than that of Halo- $\text{Na}_v1.7$ and Rab5 or LAMP1 (each

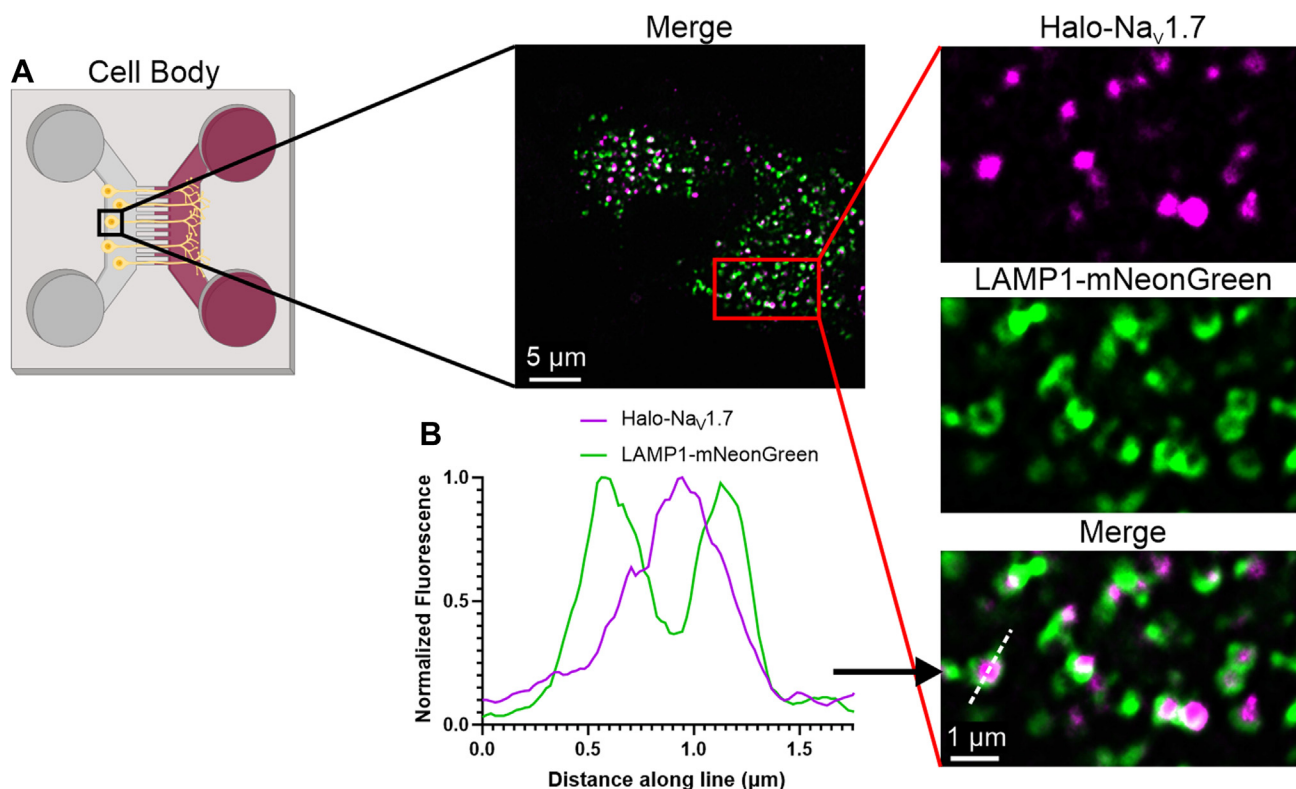


Figure 4. $\text{Na}_V1.7$ -containing endosomes are delivered to lysosomes. *A*, distal axons were labeled using cell-impermeable Halo-tag ligand JF635i, incubated for 6 h, fixed with paraformaldehyde, and then imaged using SRRF microscopy. The *black inset* shows a DRG soma, which contains both LAMP1-mNeonGreen and Halo- $\text{Na}_V1.7$. The *red inset* shows a super-resolution image of LAMP1-labeled lysosomes colocalized with Halo- $\text{Na}_V1.7$. *B*, normalized fluorescence across the *dotted line* in (*A*), *red inset*, merge, demonstrates the presence of Halo- $\text{Na}_V1.7$ within the lysosomal lumen. This pattern of labeling was observed in 30 cells from three independent cultures. DRG, dorsal root ganglion; LAMP1, lysosomal-associated membrane protein 1; Na_V , voltage-gated sodium channel; SRRF, super-resolution radial fluctuation.

endocytosis and packaging for retrograde transport. Together, these results demonstrate that Na_V channels continuously undergo endocytosis at distal axons followed by dynein-dependent retrograde transport.

$\text{Na}_V1.7$ is transported retrogradely in Rab7 endosomes and delivered to lysosomes in cell bodies

We next sought to confirm that the retrogradely transported $\text{Na}_V1.7$ puncta observed in Figure 2 are indeed endosomes and specify their stage of maturity along the early endosome, late endosome, and lysosome axis. Thus, we cotransfected DRG neurons with Halo- $\text{Na}_V1.7$ and either GFP-Rab7, EGFP-Rab5, or lysosomal-associated membrane protein 1 (LAMP1)-mNeonGreen, which are markers of late endosomes/multivesicular bodies, early endosomes, and lysosomes, respectively (25, 26). Two-color movies of axons expressing both surface-labeled Halo- $\text{Na}_V1.7$ channels that have been internalized and GFP-Rab7 demonstrate a high rate of cotransport

(colocalization over time and space) of the two proteins (Fig. 3, *A* and *D*), whereas most of the $\text{Na}_V1.7$ endosomes moved independently of Rab5 (Fig. 3, *B* and *D*) and LAMP1 (Fig. 3, *C* and *D*). When we analyzed the proportion of endosomes that were positive for both $\text{Na}_V1.7$ and individual endosome markers, a large portion of the $\text{Na}_V1.7$ endosomes that were positive for Rab7 moved in the retrograde direction, whereas most of the $\text{Na}_V1.7$ endosomes that were positive for Rab5 were stationary or moving bidirectionally. There were few $\text{Na}_V1.7$ endosomes that were positive for LAMP1, and most of those moved in the retrograde direction (Fig. 3*E*). While $\text{Na}_V1.7$ endosomes could be seen stationary or moving retrogradely, anterogradely, or bidirectionally, we were particularly interested in retrogradely moving endosomes and performed an additional subanalysis focused on this population. The majority of retrogradely moving Halo- $\text{Na}_V1.7$ endosomes were positive for Rab7 and negative for Rab5 and LAMP1 (Fig. 3*F*).

Although we detected the localization of internalized $\text{Na}_V1.7$ channels in lysosomes in the axons, these LAMP1-positive

point represents one axon, $p < 0.0001$, ANOVA with Dunnett's multiple comparisons test, error bars indicate mean \pm SD). *E*, most $\text{Na}_V1.7$ endosomes that were also positive for Rab7 were stationary (85 of 265) or moving in the retrograde direction (122 of 265), whereas most $\text{Na}_V1.7$ endosomes positive for Rab5 were stationary (34 of 89) or moving bidirectionally (43 of 89). There were few $\text{Na}_V1.7$ - and LAMP1-positive endosomes, most of which moved retrogradely (18 of 28). *F*, most $\text{Na}_V1.7$ endosomes that were moving in the retrograde direction were positive for Rab7 (101 positive of 139 total) and negative for Rab5 (19 positive of 166 total) or LAMP1 (17 positive of 68 total) (each point represents one axon, $p < 0.0001$, ANOVA with Dunnett's multiple comparisons test, error bars indicate mean \pm SD). *D–F*, N axons: Rab7 = 18, Rab5 = 20, and LAMP1 = 14, three independent cultures each. EGFP, enhanced GFP; LAMP1, lysosomal-associated membrane protein 1; MFC, microfluidic chamber; Na_V , voltage-gated sodium channel.

The fates of internalized Na_v channels in sensory neurons

vesicles were rare (Fig. 3, D and F). Next, we wanted to find out whether the internalized Na_v1.7 channels are eventually delivered to lysosomes once they arrive at the cell body. Given the thin focal plane of the spinning disk confocal microscope, retrogradely moving endosomes that arrived at the cell body tended to quickly leave the focal plane once they enter the relatively large volume of the cell body. Therefore, in order to visualize Na_v-carrying endosomes within the cell body, the cells were fixed 6 h after axonal surface labeling and then imaged using super-resolution radial fluctuations (SRRF) microscopy (27). Na_v1.7 that were retrogradely transported to the soma could be seen closely colocalized with LAMP1 (Fig. 4A). Occasionally, Na_v1.7 signal could be seen within individual lysosomal lumens (Fig. 4B).

Together, these results demonstrate that endocytosed Na_v1.7 can be observed in Rab5 early endosomes but that the endosomes mature to Rab7 late endosomes prior to initiating retrograde transport (25). Furthermore, Na_v1.7-containing endosomes leaving distal axons have not fused with lysosomes, but at least some Na_v1.7 channels are eventually delivered to lysosomes within the cell body.

Na_v1.7 endosomes contain multiple types of membrane proteins

We next sought to determine whether the Rab7 endosomes that transport Na_v1.7 away from distal axons carry only Na_v1.7 or also contain other axonal membrane proteins. To test this, we engineered multiple axonal ion channels with extracellular Halo tags or SNAP tags: SNAP-Na_v1.7, Halo-Na_v1.8, Halo-K_v7.2 (28) as well as an extracellularly tagged Halo-TrkA. SNAP tag is an enzymatic tag that functions similarly to Halo tag but has a different specific cognate ligand, enabling simultaneous use with Halo tag. We transfected DRG

neurons with SNAP-Na_v1.7 and either Halo-Na_v1.8, Halo-K_v7.2, or Halo-TrkA and then labeled surface proteins with SNAP-tag ligand JF549i and Halo-tag ligand JF635i. After waiting for endocytosis to occur (beginning approximately 40 min after the start of labeling), we observed that 75 to 80% of retrogradely moving Na_v1.7-carrying endosomes also contained Na_v1.8, K_v7.2, or TrkA (Fig. 5, A–D). These results demonstrate that late endosomes in axons do not transport one type of protein specifically but rather several proteins together.

Na_v1.7 does not undergo transcytosis

To test whether Na_v1.7 channels are distributed within sensory neurons *via* transcytosis, we utilized cell-permeable and cell-impermeable Halo-tag ligands in the MFC system. Transfected DRG cell bodies in the soma chamber were first exposed to Halo-tag ligand JF635i, labeling only channels at the cell surface, and then to Halo-tag ligand JF549, labeling channels in the cytoplasm (Fig. 6A). After labeling, distal axons expressing Halo-Na_v1.7 were identified by the presence of anterogradely trafficking vesicles with JF549 signal. Although these axons continued to transport JF549-tagged Halo-Na_v1.7 up to 4 h after labeling, JF635i fluorescence was not reliably observed moving in the anterograde direction in three independent cultures, each of which contained dozens of transfected axons (Fig. 6B). As a positive control to ensure that transcytosis occurs in our preparation and is detectable using our methodology, we carried out the same transfection, culture, and labeling protocol using cells transfected with Halo-TrkA, a protein previously shown to undergo transcytosis (29). Several hours after labeling, JF635i that had been applied to the soma compartment was seen being trafficked

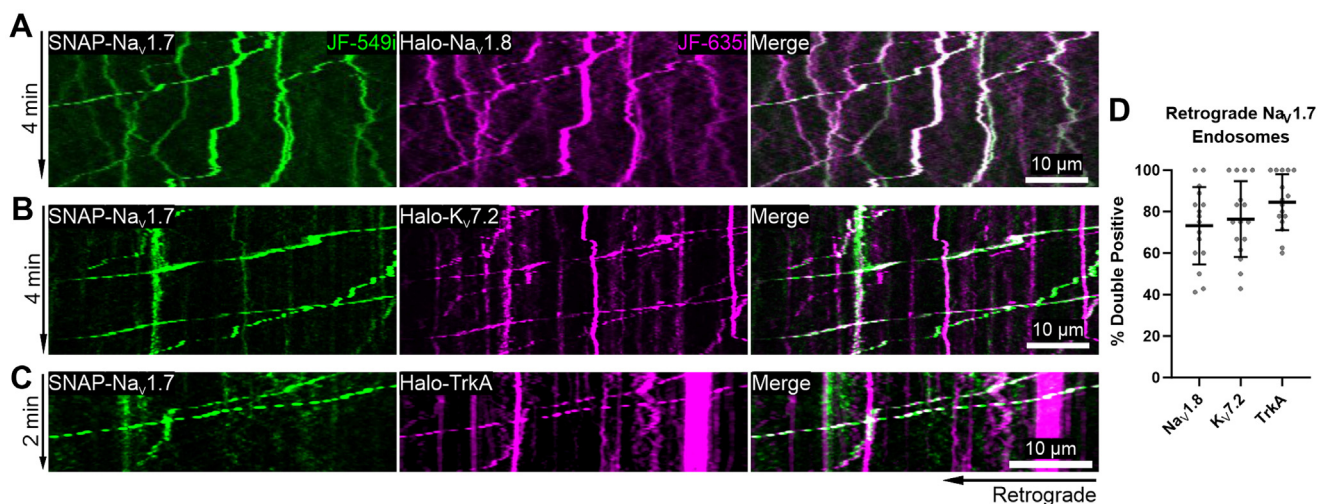


Figure 5. Endosomes carrying Na_v1.7 contain multiple types of membrane proteins. DRG neurons were transfected with SNAP-Na_v1.7 and Halo-tagged Na_v1.8 (A), K_v7.2 (B), or TrkA (C), all of which are tagged on the extracellular part of the protein. The cells were then cultured in MFCs for 5 days. Proteins at the surface of distal axons were labeled using cell-impermeable SNAP-tag ligand JF549i and Halo-tag ligand JF635i, and videos of axons were recorded in both red (JF549i, pseudocolored green) and far-red (JF635i pseudocolored magenta) channels. Axons were imaged 40 to 90 min after the start of labeling. A–C, two-color kymographs show frequent cotransport of the tagged membrane proteins. D, approximately 75 to 80% of retrogradely moving endosomes carrying Na_v1.7 also contained Na_v1.8, K_v7.2, or TrkA ($p = 0.16$, ANOVA, error bars indicate mean \pm SD; N endosomes: Na_v1.8 = 135, K_v7.2 = 118, TrkA = 119; N axons = 16 each, three independent cultures each). DRG, dorsal root ganglion; MFC, microfluidic chamber; Na_v, voltage-gated sodium channel; K_v, voltage-gated potassium channel; TrkA, tropomyosin receptor kinase A.

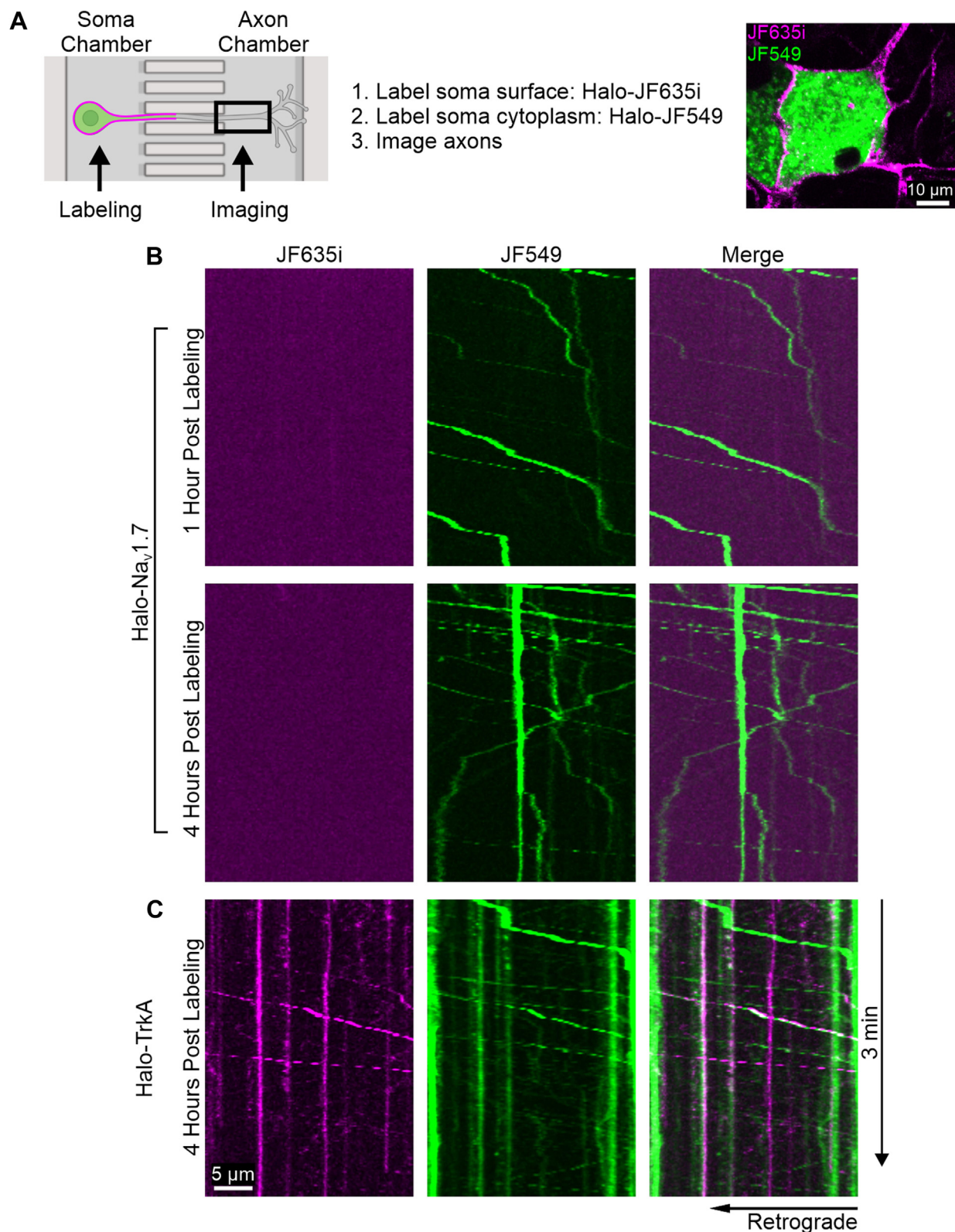


Figure 6. $Na_v1.7$ does not undergo transcytosis. Transcytosis is the process by which some proteins at the surface of a neuronal cell body or dendrites are internalized and then trafficked anterogradely to axons. DRG neurons were transfected with either Halo- $Na_v1.7$ or Halo-TrkA and cultured in MFCs for 5 days. *A*, schematic of the labeling protocol: First, Halo tag at the soma surface was labeled with cell-impermeable Halo-tag ligand JF635i, and then Halo tag within the cytoplasm was labeled with cell-permeable Halo-tag ligand JF549. Two-color movies were then recorded in the axonal chamber for up to 4 h. The *lower panel* shows a DRG cell body labeled in this manner. *B*, kymographs from axons show anterograde trafficking of Halo- $Na_v1.7$ -JF549 (*green*) 1 h (*upper panels*) and 4 h (*lower panels*) after labeling. After 1 h, JF549 is seen moving mostly in the anterograde direction, but after 4 h, it can also be seen stationary or moving retrogradely. Anterograde movement of JF635i could not be reliably detected in three independent cultures, each of which contained dozens of transfected axons. *C*, a kymograph of an axon that had been labeled as in (*A*) shows Halo-TrkA-JF635i moving anterogradely 4 h after labeling, confirming that TrkA undergoes transcytosis. Such transport was observed in at least 21 axons from three independent cultures. DRG, dorsal root ganglion; MFC, microfluidic chamber; Na_v , voltage-gated sodium channel; TrkA, tropomyosin receptor kinase A.

The fates of internalized Na_v channels in sensory neurons

anterogradely toward axonal ends, confirming that the surface-labeled Halo-TrkA had undergone transcytosis (Fig. 6C).

Na_v1.7 is preferentially recycled to the axonal membrane

Next, we investigated whether Na_v1.7 that had undergone endocytosis could be recycled back to the cell surface. To do this, we adapted a previously published cell surface protein recycling assay (30), schematized in Figure 7A. Importantly, in addition to its extracellular Halo tag, Halo-Na_v1.7 also contains a myc tag on its extracellular face, which facilitates cell-surface antibody labeling. DRG neurons were transfected with Halo-Na_v1.7, and channels at the surface of the neurons were labeled by adding an anti-Myc antibody to the live cells. Na_v1.7 at the membrane and throughout the cytoplasm were also labeled with Halo-tag ligand JF549 to facilitate identification of transfected cells (step 1). Next, the cells were returned to the incubator to allow for primary-labeled channels to undergo endocytosis (step 2). Then, the cells were labeled with a saturating concentration of Fab secondary antibody fragment conjugated to a far-red fluorophore (Fab-AF647) to label all primary-labeled channels still at the cell surface (“surface” channels, step 3). Fab fragments were used to avoid protein aggregation by secondary antibody cross-linking, though dimer formation was possible because of the bivalent nature of the primary antibody. The cells were then either kept on ice to arrest trafficking or incubated at 37 °C for 2 h to allow channel recycling to occur (step 4). Next, a saturating concentration of Fab secondary antibody fragment conjugated to a green fluorophore (Fab-AF488) was used to label any channels that had been internalized after primary labeling and then reinserted into the membrane (“recycled” channels, step 5).

Interestingly, we observed differences in behavior of channels at the surface of the soma compared with those along the proximal axons, which necessitated analyzing somas and axons separately. Generally, fewer channels were seen at the surface of somas when compared with their axons. In cells that were incubated for periods too short for recycling to occur, there were clear “surface” signals around the soma and along the axon but very weak “recycled” signals (Fig. 7B, 0 h). In contrast, cells that were incubated for 2 h at 37 °C demonstrated reduced “surface” signals at the perimeter of the cell and translocation of this signal to the cytoplasm (consistent with endocytosis) and increased “recycled” signals (Fig. 7B, 2 h). While the reduction in “surface” signal and increase in “recycled” signal between 0 and 2 h was significant along axons, the somas showed a similar trend that did not reach significance (Fig. 7, C and D).

It is possible that the appearance of the “recycled” signal in axons after 2 h of incubation could be due to secondary antibodies switching from one channel to another rather than channel trafficking. To exclude this possibility, we used two control treatments known to inhibit trafficking: incubating cells at 16 °C (31) and treating cells with the ionophore monensin (29) for the duration of the recycling step (step 4). The axons incubated at 16 °C displayed both decreased

endocytosis of “surface” channels and appearance of “recycled” channels, whereas the cells treated with monensin showed normal levels of endocytosis but decreased “recycled” channels (Fig. 7, B and C). This is consistent with 16 °C incubation inhibiting both endocytosis and recycling and monensin preferentially inhibiting recycling over endocytosis. Together, these results suggest that Na_v1.7 undergoes endocytosis in both the axon and soma but is preferentially recycled to the membrane of the axon.

Discussion

Hyperexcitability of nociceptors drives pain and is dependent on ion channel currents, which are in part dependent on levels of these channels at the cell surface, which in turn depends on regulation of the different aspects of channel trafficking. Therefore, the insights into the mechanisms of channel trafficking provided by these studies are necessary for understanding how these mechanisms might be regulated in disease and may inform efforts to modulate channel trafficking for therapeutic benefit.

Until recently, the study of Na_v channel trafficking using full-length proteins in live neurons was not possible because of dim fluorescence of existing channel constructs tagged with fluorescent proteins and the presence of a large cytoplasmic pool of Na_v channels, which precluded observing the movement of vesicles that carry a small number of channels. Instead, most previous studies of Na_v channel trafficking relied on reporter proteins fused to channel fragments, fixed immunocytochemistry, and biochemical methods (3, 32–34). However, we have developed novel tagged channels and imaging methods, which have allowed the observation of full-length sodium channel trafficking in live neurons (15, 28). In the present study, we build upon these advances to make the first real-time observations of Na_v channel retrograde trafficking. In summary, these experiments demonstrate that Na_v1.7 undergoes (1) endocytosis in distal axons, (2) preferential recycling to the membrane of axons but not somas, (3) dynein-dependent retrograde transport in Rab7 late endosomes with other axonal proteins to DRG somas, and (4) lysosomal degradation in the soma, but not transcytosis (Fig. 8).

The principal contribution of our current studies is a demonstration of which of the multiple endocytic pathways Na_v1.7 channels enter after they have been internalized. First, we show that in this experimental preparation, Na_v1.7 endocytosis is constitutive and occurs on a time scale of hours. This suggests that the population of channels at the surface of these axons has a substantial dynamic component and thus may be modulable. Furthermore, we demonstrate that a subpopulation of internalized Na_v1.7 channels enters degradative endosomes, which mature from early endosomes to late endosomes and eventually lysosomes, whereas another subpopulation is recycled to the plasma membrane. Our new strategies of tagging full-length channels and methods that enhance the signal/noise ratio in live imaging of sensory neurons have enabled studying these dynamic processes for the first time.

The fates of internalized Na_v channels in sensory neurons

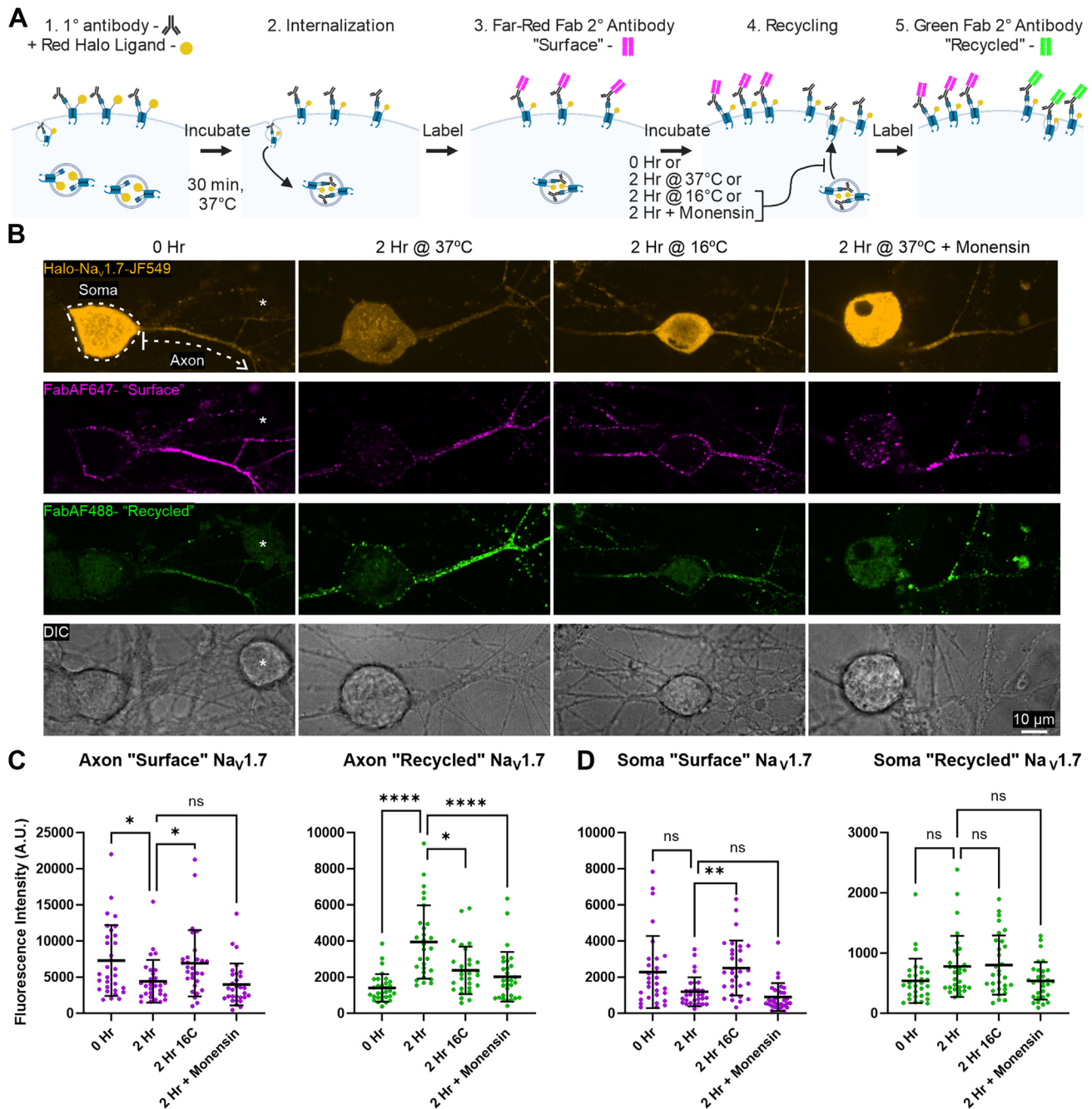


Figure 7. Internalized $Na_v1.7$ channels are recycled to the membrane of axons but not somata. DRG neurons were transfected with Halo- $Na_v1.7$ and cultured for 4 to 5 days. **A**, schematic of the surface-channel recycling assay adapted from Ref. (30). See results and methods for full descriptions of the assay. **B**, representative images of DRG somata and proximal axons, which had undergone the labeling protocol in (A). For each cell, fluorescent signals were measured at the surface of the soma and proximal portion of the axon (dotted white lines, upper left panel). The top row shows intracellular Halo- $Na_v1.7$ labeled by Halo-tag ligand JF549 (step 1: yellow). The second row shows Halo- $Na_v1.7$ labeled by Fab-AF647 (step 3: "surface"—magenta). The third row shows Halo- $Na_v1.7$, which had been endocytosed and then recycled back to the membrane to be labeled by Fab-AF488 (step 5: "recycled"—green). The bottom row shows DIC images with normal DRG morphology. Note the absence of fluorescent signals from the untransfected cell marked by the asterisk in the left column (0 h), confirming specific labeling. All images were processed and thresholded identically. **C**, the signal from $Na_v1.7$ channels labeled at the surface of axons in step 3 decreased after 2 h of incubation (with or without monensin) but not when the cells were incubated at 16 °C (left panel). The levels of recycled $Na_v1.7$ channel at the surface of axons (step 5) were low initially and increased after 2 h of incubation but not when the cells were treated with monensin or incubated at 16 °C (right panel, $N = 29$ –31 cells, each condition from three cultures, $*p < 0.01$, $****p < 0.0001$). **D**, at the surfaces of somata, similar trends were observed, but the signals were generally weaker, and most of the differences did not reach statistical significance ($N = 30$ cells each condition from three cultures, $**p < 0.01$). **C** and **D**, error bars indicate mean \pm SD. The Kruskal–Wallis test (with Dunn's correction for multiple comparisons) was used to compare each condition to the 2 h sample. DIC, differential interference contrast; DRG, dorsal root ganglion; Na_v , voltage-gated sodium channel.

These studies also contribute to understanding of the development of polarity in sensory neurons. Directional flow of information through neurons depends on the specialization

of different anatomical structures such as axons and dendrites and microdomains such as the AIS and nodes of Ranvier in myelinated fibers, which differentially concentrate specific ion

The fates of internalized Na_v channels in sensory neurons

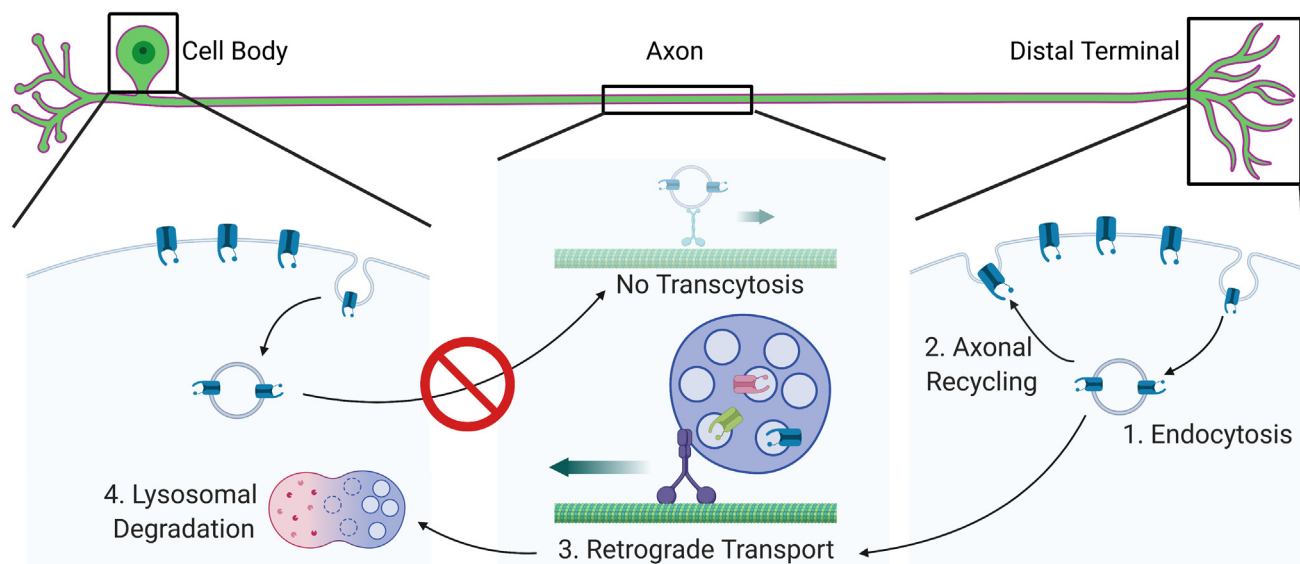


Figure 8. The fates of $\text{Na}_v1.7$ channels after endocytosis. $\text{Na}_v1.7$ undergoes (1) endocytosis in distal axons, (2) recycling to the membrane of axons but not somas, (3) dynein-dependent retrograde transport in Rab7 late endosomes with other axonal proteins to DRG somas, and (4) lysosomal degradation in the soma but not transcytosis. DRG, dorsal root ganglion; Na_v , voltage-gated sodium channel.

channels and other membrane proteins. This polarization has been reported to be established by multiple mechanisms including directed delivery, selective insertion, and endocytosis, and specific retention of proteins in different membrane domains (16, 35). Examples of these mechanisms include exclusion of vesicles carrying dendritic proteins from the axon (36), preferential direct insertion of $\text{Na}_v1.6$ to the AIS (19), and selective endocytosis of a reporter protein containing a fragment of $\text{Na}_v1.2$ from the cell body membrane and trapping within the AIS (20). However, polarized distribution of proteins in unmyelinated sensory neurons without well-defined and distinct microdomains is less well understood. Recently, we documented concentrations of $\text{Na}_v1.7$ channels at the surface of proximal axons and at distal axonal ends (15). Here, we observe a potentially novel mechanism for maintenance of this membrane specialization: selective recycling of $\text{Na}_v1.7$ to the membrane of proximal axons and not somas. Action potential firing in sensory neurons is initiated within the distal axonal ends in target tissue, which could be more than a meter away from the soma. Local recycling as demonstrated in this study is one potential mechanism to maintain the necessary density of surface sodium channels at these distal axonal ends, which is needed for an effective neuronal response to external stimuli. However, given the pseudounipolar anatomy of DRG neurons, determining the functional significance of this polarization will require further studies.

Whether internalized proteins are degraded or recycled to the membrane is dependent on complex sorting machinery, which can be influenced by multiple factors. Typically, protein ubiquitination and subsequent engagement of endosomal sorting complex required for transport complexes lead to lysosomal degradation, whereas engagement of recycling signal sequences by complexes such as retromer and retriever promote recycling (37). Thus, modifications of these ubiquitination sites and signal sequences can shift the balance of

recycling *versus* degradation (38). Furthermore, these processes can be regulated by neuronal activity; for example, transient receptor potential vanilloid 1 undergoes activity-dependent recycling in neurons (39). There is also evidence that modification of the $\text{Na}_v1.7$ binding partner CRMP2 influences $\text{Na}_v1.7$ ubiquitination and endocytosis (40). While the NEDD4-2 ubiquitinase has been shown to regulate $\text{Na}_v1.7$ endocytosis (41), neither the ubiquitinated lysine residues nor potential recycling sequences for $\text{Na}_v1.7$ are yet known. Identification of these motifs will be necessary to uncover the mechanisms that control the balance of $\text{Na}_v1.7$ degradation and recycling. Furthermore, new methods will be necessary to directly compare the relative rates of $\text{Na}_v1.7$ delivery to the lysosome *versus* recycling.

The process of transcytosis (somatic endocytosis followed by anterograde trafficking) is another potential fate of internalized membrane proteins. While TrkA has been shown to undergo transcytosis (29), other recent findings show that this pathway plays a minor role in the trafficking of two other axonal proteins, VAMP2 and NgCAM (42). While we were able to observe transcytosis of TrkA, the lack of reliable trafficking of $\text{Na}_v1.7$ by transcytosis in our system did not allow for a meaningful quantitative comparison. Thus, our conclusion on this subject is limited to a lack of observation of $\text{Na}_v1.7$ transcytosis in this system.

We also show that internalized Na_v channels are packaged together in late endosomes for retrograde transport together with other ion channels and membrane proteins, which is consistent with a previous report (43). This is perhaps unsurprising given that late endosomes arise from homotypic fusion of many early endosomes (44), which may be expected to lead to the mixing of cargos. This integrated transport is consistent with our report that multiple ion channels and axonal membrane proteins are trafficked together in the same vesicles in the anterograde direction (28). However, it is also

possible that certain axonal proteins may be handled in a more specific manner *via* earlier endocytic or recycling processes, as has been demonstrated for opioid receptors (45). In the present study, we used cell-impermeable Halo-tag ligands to label channels at the cell surface, and we were able to infer that the channels had undergone endocytosis based on their retrograde motion and colocalization with endocytic markers. However, this tagging method does not allow us to pinpoint the moment at which channels are internalized. Observing early endocytic processes in small and crowded distal axons will require new imaging strategies. Future experiments might utilize a combination of acid-sensitive or acid-activated fluorophores to observe individual endocytic events as well as endosome fusion and sorting and channel recycling in the crowded distal axon terminal.

To our knowledge, this study presents the first detailed observations of endocytosis and retrograde trafficking of a full-length Na_v channel in live cells. However, there are multiple limitations to consider. First, our reductionist model system consists of neurons developing without their normal milieu including myelin, glial cells, target cells, and extracellular matrix, which may influence channel behavior and stability at the cell membrane (46). We interpret the observed behavior as neuron intrinsic. Future studies could recapitulate components of *in vivo* complexity by observing Na_v channel behavior in cocultures of neurons with other cell types. Second, it is possible that overexpression of exogenous Na_v1.7 and other tagged proteins could cause mislocalization compared with native proteins. However, our observations that internalized Na_v1.7 is trafficked independently of Rab5 and LAMP-1 in axons suggests that overexpression does not cause nonspecific labeling of retrograde vesicles. A final caveat is that the Na_v1.7 constructs used in these studies were tagged on the extracellular face of the channel by addition of the transmembrane domain of the Na_vβ4 subunit, which could potentially influence trafficking of the channel (47). However, since Na_v1.7 and the Na_vβ4 subunits are normally covalently linked by disulfide bonds, we reason that having them also linked together as a fusion protein would not meaningfully change their interaction. Furthermore, there is evidence that, unlike other Na_vβ subunits, Na_vβ4 does not influence Na_v α subunit trafficking (48, 49).

The burden of pain is substantial, and current pain treatments can be ineffective and addictive (50–53). Na_v1.7 is a promising target for pain therapy because of its genetic validation in humans, and preferential expression in peripheral sensory neurons, which suggest that interfering with its function, may alleviate pain without causing addiction (10, 11). While ongoing efforts to target Na_v1.7 for pain treatment have attempted to interfere with channel function, an alternative strategy is to modulate channel trafficking to and from the cell membrane (12). However, there are many potential mechanisms involved in channel trafficking, some of which may be more amenable to therapeutic intervention. Here, we identify pathways of endocytic Na_v trafficking, which could potentially be targeted for treatment of pain. There is precedent for modulation of ion channel trafficking as a therapeutic strategy.

For example, the antiarrhythmic agent quinidine increases the endocytosis of K_v1.5 (54). Furthermore, there is evidence that gabapentinoids decrease pain by interfering with the recycling of voltage-gated calcium channel subunits (55). Thus, interfering with Na_v1.7 recycling presents a potential therapeutic strategy for pain.

In conclusion, these studies provide the first observations of dynein-dependent retrograde trafficking of a full-length Na_v channel in live neurons, demonstrating ongoing endocytosis and sorting into degradative endosomes. We uncover various fates of Na_v1.7 channels after endocytosis, finding that some are delivered to the lysosomal compartment in cell bodies and that these channels do not appear to undergo transcytosis. Interestingly, we observe that Na_v1.7 channels undergo recycling to axonal membranes, but not to somas, demonstrating a potential mechanism by which neurons maintain polarity. Promoting endocytosis and degradation or reducing recycling of Na_v channels represent potential therapeutic strategies for the treatment of disorders of excitability, including pain.

Experimental procedures

DNA constructs

The construction of plasmids encoding Halo-Na_v1.7, SNAP-Na_v1.7, Halo-Na_v1.8, and Halo-K_v7.2 was described previously (28). The codon-optimized Halo-Na_v1.7 construct followed the protocol for the construction of the noncodon-optimized Halo-Na_v1.7 (15) and was described previously (28). Briefly, the final construct topology is in order from the N terminus: 1 to 30 amino acids β4 signal peptide, 3× myc tag (EQKLISEEDL), Halo-tag enzyme (297 amino acids) (Promega), 3× hemagglutinin tag (YPYDVPDYA), 21 amino-acid transmembrane segment (β4 163–183), 7 amino-acid linker (SGLRSAT), hNa_v1.7-R. SNAP-Na_v1.7 was derived from the noncodon-optimized Halo-Na_v1.7 construct (15) by replacing the Halo tag with the 182 amino acid SNAP_f (New England Biolabs) using megamutagenesis.

The codon-optimized human Na_v1.8 construct (pcDNA5-SCN10A) was purchased from Genionics and previously reported (56). Codon-optimized Halo-Na_v1.8 was created in a protocol identical to that used to create the Halo-Na_v1.7.

EGFP-Rab5 (plasmid 49888; Addgene) was a gift from M. Scidmore (57). GFP-Rab7 (plasmid 12605; Addgene) was a gift from R. Pagano (58). LAMP1-mNeonGreen (plasmid #98882; Addgene) was a gift from T.W.J. Gadella (59).

pCMV5-TrkA (plasmid 15002) was obtained from Addgene as a gift from Raymond Birge. This construct had a mutation V289L, which was corrected using QuikChange Lightning site-directed mutagenesis (Agilent Technologies). Halo-TrkA was created by inserting 297 amino-acid Halo-tag enzyme (Promega) after the signal peptide of TrkA and flanked by 2 amino acid-GlyAla using megamutagenesis.

Primary DRG neuron culture and transfection

Animal studies followed a protocol approved by the Veterans Administration Connecticut Healthcare System Institutional Animal Care and Use Committee.

The fates of internalized Na_v channels in sensory neurons

DRG neurons were isolated from 2- to 4-day-old Sprague–Dawley rats as described previously (60). Briefly, dissected DRGs were first incubated at 37 °C for 20 min in complete saline solution (137 mM NaCl, 5.3 mM KCl, 1 mM MgCl₂, 25 mM sorbitol, 3 mM CaCl₂, and 10 mM Hepes [pH 7.2], adjusted with NaOH) and supplemented with 0.6 mM EDTA and collagenase A (1.5 mg/ml; Roche). Rat DRGs were then incubated for 20 min at 37 °C in complete saline solution containing collagenase D (1.5 mg/ml; Roche) and papain (30 U/ml; Worthington Biochemical). DRGs were centrifuged and triturated in 1 ml of DRG culture medium (Dulbecco's modified Eagle's medium/F12 [1:1] with penicillin [100 U/ml], streptomycin [0.1 mg/ml; Life Technologies], 2 mM L-glutamine, and 10% fetal bovine serum [Hyclone] containing bovine serum albumin [1.5 mg/ml; low endotoxin; Sigma–Aldrich] and trypsin inhibitor [1.5 mg/ml; Sigma–Aldrich]). The cell suspension was filtered through a 70 µm nylon mesh cell strainer (Becton Dickinson) to remove debris, and the mesh was then washed once with 1 ml of DRG culture medium.

Transfection of DRG neurons was performed as previously described (15, 60). Briefly, DRG neurons were pelleted (200g, 3 min) and gently resuspended with 20 µl of Nucleofector solution, and then the cell suspension was mixed with DNA. Neurons were transfected using Nucleofector IIS Electroporator (Lonza) using protocol SCN-BNP 6 and Amaxa SCN Nucleofector reagents (VSP1-1003; Lonza). Amounts of DNA transfected were Halo-Na_v1.7 (1.5 µg), EGFP-Rab5 (0.2 µg), GFP-Rab7 (0.2 µg), SNAP-Na_v1.7 (1.5 µg), Halo-Na_v1.8 (1.5 µg), Halo-K_v7.2 (0.2 µg), Halo-TrkA (0.1 µg), and LAMP1-mNeonGreen (0.05 µg). After electroporation, 100 µl of calcium-free Dulbecco's modified Eagle's medium (37 °C) was added, and cells were incubated at 37 °C for 5 min in a 95% air/5% CO₂ (v/v) incubator to allow neurons to recover. The cell mixture was then diluted with DRG medium containing bovine serum albumin (1.5 mg/ml) and trypsin inhibitor (1.5 mg/ml). Rat DRGs were carefully seeded onto 35 mm glass bottom dishes coated with poly-D-lysine/Laminin (MatTek) or onto the somatic chamber of MFCs. DRGs cultured on coverslips were incubated at 37 °C for 45 min to allow DRG neurons to attach. Then, DRG medium was added to each well to a final volume of 1.5 ml (in 35 mm glass bottom dishes) or about 350 µl (in somatic chamber of MFCs) individually. DRG neurons were maintained at 37 °C in a 95% air/5% CO₂ (v/v) incubator before use.

MFCs

As described previously (15), MFCs (DOC450, two-chamber 450 µm groove; Xona Microfluidics) were bound to glass bottom dishes according to the manufacturer's instructions. Briefly, MFCs were soaked in ethanol for 1 min and then air dried before being placed on 50 mm glass bottom dishes (P50G-1.55-30-F; MatTek) that were coated with poly-L-lysine (0.5 mg/ml) overnight at 37 °C. The glass surface was washed twice with sterile double-distilled water and then air dried in a sterile hood. The dishes were then coated with laminin (10 mg/ml) for at least 2 h at 37 °C, excess laminin was

aspirated, and the dishes were air dried under the hood before MFCs were adhered. Transfected DRG neuron suspension was applied in the soma chamber containing DRG medium with growth factors (50 ng/mg) (nerve growth factor and glial cell line–derived neurotrophic factor from PeproTech), and 2× growth factors (100 ng/mg) were added to the axonal chamber. Medium was changed to serum-free medium in both chambers after 24 h (Neurobasal medium supplemented with 2% B27, 1% penicillin/streptomycin, same 1:2 ratio of nerve growth factor, glial cell line–derived neurotrophic factor in soma and axonal chambers), and 1 µM uridine/5-fluoro-2-deoxyuridine was added to inhibit the growth of fibroblasts and glia.

Imaging system

As described previously (15), images were acquired using an Andor Dragonfly spinning disk confocal platform together with a Nikon Eclipse Ti Fluorescence microscope. Images were taken using an Andor iXon 888 electron multiplying charge-coupled device camera through a Plan Apo Lambda 60× (numerical aperture = 1.4 oil objective), except where otherwise stated. The light source is an Andor Integrated Laser Engine containing 150 mW 488 nm, 150 mW 561 nm, and 140 mW 637 nm solid state lasers. Emission filters include 525/50, 600/50, and 700/75 nm. The Nikon perfect focus system was used to maintain focus during time-lapse experiments. Andor Fusion software (Oxford Instruments) was used to control the system and acquire images.

Time-lapse imaging

All Halo-tag ligand– and SNAP-tag ligand–conjugated Janelia Fluor labels were generous gifts of L.D. Lavis and J.B. Grimm (Janelia Research Campus).

All live-cell experiments were performed at 37 °C using a stage incubator (Tokai Hit). During labeling and imaging, neurons were kept in DRG neuronal imaging saline (NIS) containing 136 mM NaCl, 3 mM KCl, 1 mM MgSO₄, 2.5 mM CaCl₂, 0.15 mM NaH₂PO₄, 0.1 mM ascorbic acid, 20 mM Hepes, and 8 mM dextrose (pH 7.4) with NaOH (adjusted to 320 mOsm/l).

DRG neurons transfected with Halo-Na_v1.7 were cultured in MFCs for 5 to 7 days. Cell-impermeable Halo-tag ligand JF635i (100 nM) was added to the somatic chamber for 15 min and then removed by washing the chamber 3× with NIS.

For time lapses of Na_v channel trafficking (Fig. 2), multiple fields of view containing distal axons with labeled Na_v1.7 channels were selected and imaged sequentially, one image per field, every ~4 s for 900 frames. Cells that were treated with ciliobrevin D (20 µM final concentration, stock solution was made in dimethyl sulfoxide immediately prior to use; Millipore) were exposed from the start of labeling and throughout the experiment.

Kymograph generation and trafficking analysis

Kymographs were generated using KymographClear and analyzed using KymographDirect (61). Movies acquired using

the methods described previously were opened in ImageJ (NIH), and the KymographClear toolset was used to create kymographs of selected axons. Specifically, axons were traced manually using a segmented line, and KymographClear extracts the signal under that line and converts it into a two-dimensional image with distance on the x -axis and time on the y -axis. Only axons that were separate from other axons were analyzed.

Vesicle trajectories (excluding the initial stationary period of endosomes and any additional stops) were manually traced in ImageJ and recorded by KymographClear. Traces were then loaded into KymographDirect, from which velocity measurements were extracted. The times at which individual endosomes were first observed moving in the retrograde direction was recorded, and these were grouped into 10 min bins according to how much time had elapsed since the start of labeling.

Cotrafficking assays

DRG neurons transfected with Halo- and SNAP- or fluorescent protein-tagged constructs were cultured in MFCs for 5 to 7 days. Cell-impermeable Halo-tag ligand JF635i (100 nM) with or without SNAP-tag ligand JF549i (100 nM) were added to the somatic chamber for 15 min (in experiments with Halo-tag only) or 30 min (for experiments with Halo tag and SNAP tag) and then removed by washing the chamber 3 \times with NIS. Fields of view containing axons expressing both tagged proteins were selected, and two-color time lapses were recorded with a frame rate of 2 s for 10 min. Since few retrogradely moving endosomes are visible in the first 30 min after the start of surface labeling, axons were imaged 40 to 90 min after the start of labeling. Axons were selected for analysis if there was at least one moving vesicle of each construct visible in the axon, indicating that the neuron had been transfected with both constructs. Kymographs of these axons were created, and vesicles were categorized as either single positive for either construct or double positive by eye. Vesicles categorized as positive for both $\text{Na}_v1.7$ channels, and endosome or lysosome markers were further characterized as moving entirely retrogradely, entirely anterogradely, bidirectionally (at least 5 μm motion in both directions), or stationary (less than 5 μm motion in either direction).

Super-resolution imaging

SRRF microscopy was performed using the imaging system described previously together with the Andor SRRF-Stream software (Oxford Instruments). SRRF images were taken using an SF Apo TIRF 100 \times (numerical aperture, 1.49) oil objective and 1.5 \times optical magnification. SRRF acquisition settings were 100 frames, 4 \times radiality magnification, and 2 px ring radius.

Transcytosis assay

DRG neurons were transfected with Halo- $\text{Na}_v1.7$ or Halo-TrkA plasmids and cultured in MFCs as aforementioned. First, cell-impermeable Halo-tag ligand JF635i (100 nM) was added to the soma chamber for 15 min, then washed away, and replaced with

cell-permeable Halo-tag ligand JF549 (100 nM) for 15 min. The cells were then placed in the stage-top incubator, and multicolor time lapses were recorded of axons at multiple time points.

Recycling assay

The assay was adapted from a published study (30). Rat DRG neurons were harvested as previously and cultured in 35mm glass bottom dishes coated with poly-D-lysine/laminin (MatTek) for 4 to 5 days. The cell media were replaced with NIS three times before the cells were blocked with 5% donkey serum in NIS for 15 min. All subsequent antibody labeling occurred in the presence of 5% donkey serum. The cells were then labeled with goat anti-Myc primary antibody (ab9132; Abcam; 1:250 dilution) and Halo-tag ligand JF549 (100 nM) for 30 min on ice. Primary antibody was then washed away three times on ice, before the cells were returned to the 37 $^\circ\text{C}$ incubator for 30 min. Cells were then labeled with the first secondary antibody fragment (donkey antigoat Fab-AF647; Jackson ImmunoResearch, 1:250 dilution) for 30 min on ice, followed by three washes on ice. Cells were then either kept on ice (0 h incubation), incubated at 37 $^\circ\text{C}$ for 2 h, incubated at 37 $^\circ\text{C}$ for 2 h in the presence of monensin (Thermo Fisher; 2 μM), or incubated at 16 $^\circ\text{C}$ for 2 h. Cells were then labeled with the second secondary antibody fragment (donkey antigoat Fab-AF488; Jackson ImmunoResearch, 1:250 dilution) for 30 min on ice, followed by three washes on ice, and finally fixed in 4% paraformaldehyde for 15 min on ice and mounted with FluoroSave Reagent (Calbiochem).

Cells were imaged using the Andor Dragonfly Spinning Disk confocal microscope described previously. Cells expressing Halo- $\text{Na}_v1.7$ channels were identified by Halo-tag ligand JF549 fluorescence, and confocal z -stacks were taken in green, red, and far-red channels (slices every 1.5 μm , encompassing the entire axon and soma). Image stacks were processed and analyzed using ImageJ. For analysis of fluorescence on the surface of somas, the z -slice in which the surface of the soma was most clear was selected, and the fluorescence at the membrane was measured using a 1 μm wide line encompassing the circumference of the cell. Since axons rarely lie in the plane of a single z -slice, max-intensity projections of the stacks were made in order to visualize the length of the axon within the field of view. Fluorescence was measured using a 1 μm wide line tracing the 45 μm of axon proximal to the soma. Background signal was measured and subtracted for each channel in each image.

Image and statistical analysis

Images were processed using either ImageJ or Imaris (Oxford Instruments). Images that are linked or compared with each other were processed identically and displayed with the same maximum and minimum pixel values and gamma adjustments. Graphs were formatted, and statistical analysis was performed using GraphPad Prism (GraphPad Software, Inc; specific tests are indicated in the figure legends). Grouped data are displayed with mean \pm SD. Schematics were created with BioRender.com.

Data availability

All information necessary to evaluate the findings of the article are included in the article. Additional data can be provided from the authors upon request. Further information and requests should be directed to the lead contact, Sulayman D. Dib-Hajj (sulayman.dib-hajj@yale.edu).

Acknowledgments—We thank Daniel Sozniak and Peng Zhao for technical assistance. We thank Elizabeth Akin and Shawn Ferguson for helpful discussions and comments on the article. We thank David Zenisek, Emile Boulpaep, Craig Crews, Angeliki Louvi, Fred Gorelick, and Reiko Fitzsimonds for helpful discussions. We thank Luke Lavis and Jonathan Grimm for the JaneliaFluors and helpful discussions. The Center for Neuroscience & Regeneration Research is a Collaboration of the Paralyzed Veterans of America with Yale University.

Author contributions—G. P. H.-R. conceptualization; G. P. H.-R. methodology; S. T. software; G. P. H.-R. and S. T. formal analysis; G. P. H.-R. investigation; S. L. and F. B. D.-H. resources; G. P. H.-R. writing—original draft; S. T., S. G. W., and S. D. D.-H. writing—review & editing; G. P. H.-R. visualization; S. G. W. and S. D. D.-H. supervision; G. P. H.-R., S. G. W., and S. D. D.-H. funding acquisition.

Funding and additional information—This work was supported by Merit Review Award B9253-C and BX004899 from the US Department of Veterans Affairs Rehabilitation Research and Development Service and Biomedical Laboratory Research and Development Service, respectively (to S. G. W. and S. D.-H.). G. P. H.-R. is supported by the National Institute of Neurological Disorders and Stroke/National Institutes of Health (grant no.: 1F31NS122417-01). G.P.H.-R. and S.T. are supported by National Institutes of Health/National Institute of General Medical Sciences Medical Scientist Training Program T32GM007205. The content is solely the responsibility of the authors and does not necessarily represent the official views of the National Institutes of Health.

Conflict of interest—The authors declare that they have no conflicts of interest with the contents of this article.

Abbreviations—The abbreviations used are: AIS, axon initial segment; DRG, dorsal root ganglion; LAMP1, lysosomal-associated membrane protein 1; MFC, microfluidic chamber; Na_v, voltage-gated sodium channel; NIS, neuronal imaging saline; SRRF, super-resolution radial fluctuation.

References

1. Waxman, S. G., and Zamponi, G. W. (2014) Regulating excitability of peripheral afferents: emerging ion channel targets. *Nat. Neurosci.* **17**, 153–163
2. Catterall, W. A., Goldin, A. L., and Waxman, S. G. (2005) International union of pharmacology. XLVII. Nomenclature and structure-function relationships of voltage-gated sodium channels. *Pharmacol. Rev.* **57**, 397–409
3. Black, J. A., Frézel, N., Dib-Hajj, S. D., and Waxman, S. G. (2012) Expression of Nav1.7 in DRG neurons extends from peripheral terminals in the skin to central preterminal branches and terminals in the dorsal horn. *Mol. Pain* **8**, 1744–8069
4. Black, J., Dib-Hajj, S., McNabola, K., Jeste, S., Rizzo, M., Kocsis, J., et al. (1996) Spinal sensory neurons express multiple sodium channel α -subunit mRNAs. *Mol. Brain Res.* **43**, 117–131

5. Nassar, M. A., Stirling, L. C., Forlani, G., Baker, M. D., Matthews, E. A., Dickenson, A. H., et al. (2004) Nociceptor-specific gene deletion reveals a major role for Nav1.7 (PN1) in acute and inflammatory pain. *Proc. Natl. Acad. Sci. U. S. A.* **101**, 12706–12711
6. Alexandrou, A. J., Brown, A. R., Chapman, M. L., Estacion, M., Turner, J., Mis, M. A., et al. (2016) Subtype-selective small molecule inhibitors reveal a fundamental role for Nav1.7 in nociceptor electrogenesis, axonal conduction and presynaptic Release. *PLoS One* **11**, e0152405
7. Grubinska, B., Chen, L., Alsalous, M., Rampal, N., Matson, D., Yang, C., et al. (2019) Rat Nav1.7 loss-of-function genetic model: deficient nociceptive and neuropathic pain behavior with retained olfactory function and intra-epidermal nerve fibers. *Mol. Pain* **15**, 1744806919881846
8. Cummins, T. R., Howe, J. R., and Waxman, S. G. (1998) Slow closed-state inactivation: a novel mechanism underlying Ramp currents in cells expressing the hNE/PN1 sodium channel. *J. Neurosci.* **18**, 9607–9619
9. McDermott, L. A., Weir, G. A., Themistocleous, A. C., Segerdahl, A. R., Blesneac, I., Baskozos, G., et al. (2019) Defining the functional role of Nav1.7 in human nociception. *Neuron* **101**, 905–919
10. Bennett, D. L., Clark, A. J., Huang, J., Waxman, S. G., and Dib-Hajj, S. D. (2019) The role of voltage-gated sodium channels in pain signaling. *Physiol. Rev.* **99**, 1079–1151
11. Dib-Hajj, S. D., and Waxman, S. G. (2019) Sodium channels in human pain disorders: genetics and pharmacogenomics. *Annu. Rev. Neurosci.* **42**, 87–106
12. Alsalous, M., Higerd, G. P., Effraim, P. R., and Waxman, S. G. (2020) Status of peripheral sodium channel blockers for non-addictive pain treatment. *Nat. Rev. Neurol.* **16**, 689–705
13. Mulcahy, J. V., Pajouhesh, H., Beckley, J. T., Delwig, A., Du Bois, J., and Hunter, J. C. (2019) Challenges and opportunities for therapeutics targeting the voltage-gated sodium channel isoform Nav1.7. *J. Med. Chem.* **62**, 8695–8710
14. Estadella, I., Pedrós-Gámez, O., Colomer-Molera, M., Bosch, M., Sorkin, A., and Felipe, A. (2020) Endocytosis: a turnover mechanism controlling ion channel function. *Cells* **9**, 1833
15. Akin, E. J., Higerd, G. P., Mis, M. A., Tanaka, B. S., Adi, T., Liu, S., et al. (2019) Building sensory axons: delivery and distribution of Nav1.7 channels and effects of inflammatory mediators. *Sci. Adv.* **5**, eaax4755
16. Horton, A. C., and Ehlers, M. D. (2003) Neuronal polarity and trafficking. *Neuron* **40**, 277–295
17. Roney, J. C., Cheng, X.-T., and Sheng, Z.-H. (2022) Neuronal endolysosomal transport and lysosomal functionality in maintaining axonostasis. *J. Cell Biol.* **221**, e202111077
18. Rasband, M. N. (2010) The axon initial segment and the maintenance of neuronal polarity. *Nat. Rev. Neurosci.* **11**, 552–562
19. Akin, E. J., Solé, L., Dib-Hajj, S. D., Waxman, S. G., and Tamkun, M. M. (2015) Preferential targeting of Nav1.6 voltage-gated Na⁺ channels to the axon initial segment during development. *PLoS One* **10**, e0124397
20. Fache, M.-P., Moussif, A., Fernandes, F., Giraud, P., Garrido, J. J., and Dargent, B. N. D. (2004) Endocytotic elimination and domain-selective tethering constitute a potential mechanism of protein segregation at the axonal initial segment. *J. Cell Biol.* **166**, 571–578
21. Jonker, C. T. H., Deo, C., Zager, P. J., Tkachuk, A. N., Weinstein, A. M., Rodriguez-Boulan, E., et al. (2020) Accurate measurement of fast endocytic recycling kinetics in real time. *J. Cell Sci.* **133**, jcs231225
22. Ross, J. L., Wallace, K., Shuman, H., Goldman, Y. E., and Holzbaur, E. L. F. (2006) Processive bidirectional motion of dynein–dynactin complexes *in vitro*. *Nat. Cell Biol.* **8**, 562–570
23. King, S. J., and Schroer, T. A. (2000) Dynactin increases the processivity of the cytoplasmic dynein motor. *Nat. Cell Biol.* **2**, 20–24
24. Chowdary, P. D., Che, D. L., Zhang, K., and Cui, B. (2015) Retrograde NGF axonal transport—motor coordination in the unidirectional motility Regime. *Biophysical J.* **108**, 2691–2703
25. Rink, J., Ghigo, E., Kalaidzidis, Y., and Zerial, M. (2005) Rab conversion as a mechanism of progression from early to late endosomes. *Cell* **122**, 735–749
26. Ye, M., Lehigh, K. M., and Ginty, D. D. (2018) Multivesicular bodies mediate long-range retrograde NGF-TrkA signaling. *eLife* **7**, e33012

27. Gustafsson, N., Culley, S., Ashdown, G., Owen, D. M., Pereira, P. M., and Henriques, R. (2016) Fast live-cell conventional fluorophore nanoscopy with ImageJ through super-resolution radial fluctuations. *Nat. Commun.* **7**, 12471
28. Higerd-Rusli, G. P., Alsaloum, M., Tyagi, S., Sarveswaran, N., Estacion, M., Dib-Hajj, F., *et al.* (2022) Depolarizing Na_v and hyperpolarizing KV channels are co-trafficked in sensory neurons. *J Neurosci* **42**, 4794–4811
29. Ascano, M., Richmond, A., Borden, P., and Kuruvilla, R. (2009) Axonal targeting of Trk receptors via transcytosis regulates sensitivity to Neurotrophin responses. *J. Neurosci.* **29**, 11674–11685
30. Zadeh, A. D., Xu, H., Loewen, M. E., Noble, G. P., Steele, D. F., and Fedida, D. (2008) Internalized Kv1.5 traffics via Rab-dependent pathways. *J. Physiol.* **586**, 4793–4813
31. Deutsch, E., Weigel, A. V., Akin, E. J., Fox, P., Hansen, G., Haberkorn, C. J., *et al.* (2012) Kv2.1 cell surface clusters are insertion platforms for ion channel delivery to the plasma membrane. *Mol. Biol. Cell* **23**, 2917–2929
32. Garrido, J. J., Fernandes, F., Giraud, P., Mouret, I., Pasqualini, E., Fache, M. P., *et al.* (2001) Identification of an axonal determinant in the C-terminus of the sodium channel Nav1.2. *EMBO J.* **20**, 5950–5961
33. Barry, J., Gu, Y., Jukkola, P., O'Neill, B., Gu, H., Mohler, P. J., *et al.* (2014) Ankyrin-G directly binds to Kinesin-1 to transport voltage-gated Na⁺ channels into axons. *Dev. Cell* **28**, 117–131
34. Su, Y. Y., Ye, M., Li, L., Liu, C., Pan, J., Liu, W. W., *et al.* (2013) KIF5B promotes the forward transport and axonal function of the voltage-gated sodium channel Nav1.8. *J. Neurosci.* **33**, 17884–17896
35. Solé, L., and Tamkun, M. M. (2020) Trafficking mechanisms underlying Nav channel subcellular localization in neurons. *Channels (Austin)* **14**, 1–17
36. Al-Bassam, S., Xu, M., Wandless, T. J., and Arnold, D. B. (2012) Differential trafficking of transport vesicles contributes to the localization of dendritic proteins. *Cell Rep.* **2**, 89–100
37. Cullen, P. J., and Steinberg, F. (2018) To degrade or not to degrade: mechanisms and significance of endocytic recycling. *Nat. Rev. Mol. Cell Biol.* **19**, 679–696
38. Cao, T. T., Deacon, H. W., Reczek, D., Bretscher, A., and Von Zastrow, M. (1999) A kinase-regulated PDZ-domain interaction controls endocytic sorting of the β₂-adrenergic receptor. *Nature* **401**, 286–290
39. Tian, Q., Hu, J., Xie, C., Mei, K., Pham, C., Mo, X., *et al.* (2019) Recovery from tachyphylaxis of TRPV1 coincides with recycling to the surface membrane. *Proc. Natl. Acad. Sci. U. S. A.* **116**, 5170–5175
40. Dustrude, E. T., Moutal, A., Yang, X., Wang, Y., Khanna, M., and Khanna, R. (2016) Hierarchical CRMP2 posttranslational modifications control Nav1.7 function. *Proc. Natl. Acad. Sci. U. S. A.* **113**, E8443–E8452
41. Laedermann, C. J., Cachemaille, M., Kirschmann, G., Pertin, M., Gosselein, R.-D., Chang, I., *et al.* (2013) Dysregulation of voltage-gated sodium channels by ubiquitin ligase NEDD4-2 in neuropathic pain. *J. Clin. Invest.* **123**, 3002–3013
42. Nabb, A. T., and Bentley, M. (2022) NgCAM and VAMP2 reveal that direct delivery and dendritic degradation maintain axonal polarity. *Mol. Biol. Cell* **33**, ar3
43. Bekku, Y., and Salzer, J. L. (2020) Independent anterograde transport and retrograde cotransport of domain components of myelinated axons. *J. Cell Biol.* **219**, e201906071
44. Brandhorst, D., Zwilling, D., Rizzoli, S. O., Lippert, U., Lang, T., and Jahn, R. (2006) Homotypic fusion of early endosomes: SNAREs do not determine fusion specificity. *Proc. Natl. Acad. Sci. U. S. A.* **103**, 2701–2706
45. Jullié, D., Stoeber, M., Sibarita, J.-B., Zieger, H. L., Bartol, T. M., Arttamangkul, S., *et al.* (2020) A discrete presynaptic vesicle cycle for neuro-modulator receptors. *Neuron* **105**, 663–677.e8
46. Dityatev, A., Seidenbecher, C. L., and Schachner, M. (2010) Compartmentalization from the outside: the extracellular matrix and functional microdomains in the brain. *Trends Neurosci.* **33**, 503–512
47. Hull, J. M., and Isom, L. L. (2018) Voltage-gated sodium channel β subunits: the power outside the pore in brain development and disease. *Neuropharmacology* **132**, 43–57
48. Miyazaki, H., Oyama, F., Inoue, R., Aosaki, T., Abe, T., Kiyonari, H., *et al.* (2014) Singular localization of sodium channel β₄ subunit in unmyelinated fibres and its role in the striatum. *Nat. Commun.* **5**, 5525
49. Laedermann, C., Syam, N., Decosterd, I., and Abriel, H. (2013) β₁- and β₃- voltage-gated sodium channel subunits modulate cell surface expression and glycosylation of Nav1.7 in HEK293 cells. *Front. Cell Neurosci.* **7**, 137
50. Benyamin, R., Trescot, A. M., Datta, S., Buenaventura, R., Adlaka, R., Sehgal, N., *et al.* (2008) Opioid complications and side effects. *Pain Physician* **11**, S105–120
51. Fayaz, A., Croft, P., Langford, R., Donaldson, L., and Jones, G. (2016) Prevalence of chronic pain in the UK: a systematic review and meta-analysis of population studies. *BMJ Open* **6**, e010364
52. Gaskin, D. J., and Richard, P. (2012) The economic costs of pain in the United States. *J. Pain* **13**, 715–724
53. Staahl, C., Olesen, A. E., Andresen, T., Arendt-Nielsen, L., and Drewes, A. M. (2009) Assessing efficacy of non-opioid analgesics in experimental pain models in healthy volunteers: an updated review. *Br. J. Clin. Pharmacol.* **68**, 322–341
54. Schumacher, S. M., McEwen, D. P., Zhang, L., Arendt, K. L., Van Genderen, K. M., and Martens, J. R. (2009) Antiarrhythmic drug-induced internalization of the atrial-specific K channel Kv1.5. *Circ. Res.* **104**, 1390–1398
55. Tran-Van-Minh, A., and Dolphin, A. C. (2010) The 2 ligand gabapentin inhibits the Rab11-dependent recycling of the calcium channel subunit 2-2. *J Neurosci* **30**, 12856–12867
56. Faber, C. G., Lauria, G., Merkies, I. S. J., Cheng, X., Han, C., Ahn, H.-S., *et al.* (2012) Gain-of-function Nav1.8 mutations in painful neuropathy. *Proc. Natl. Acad. Sci. U. S. A.* **109**, 19444–19449
57. Rzomp, K. A., Scholtes, L. D., Briggs, B. J., Whittaker, G. R., and Scidmore, M. A. (2003) Rab GTPases are recruited to chlamydial inclusions in both a species-dependent and species-independent manner. *Infect. Immun.* **71**, 5855–5870
58. Choudhury, A., Dominguez, M., Puri, V., Sharma, D. K., Narita, K., Wheatley, C. L., *et al.* (2002) Rab proteins mediate Golgi transport of caveola-internalized glycosphingolipids and correct lipid trafficking in Niemann-Pick C cells. *J. Clin. Invest.* **109**, 1541–1550
59. [preprint] Chertkova, A. O., Mastop, M., Postma, M., van Bommel, N., van der Niet, S., Batenburg, K. L., *et al.* (2020) Robust and bright genetically encoded fluorescent markers for highlighting structures and compartments in mammalian cells. *bioRxiv*. <https://doi.org/10.1101/160374>
60. Dib-Hajj, S. D., Choi, J. S., Macala, L. J., Tyrrell, L., Black, J. A., Cummins, T. R., *et al.* (2009) Transfection of rat or mouse neurons by biolistics or electroporation. *Nat. Protoc.* **4**, 1118–1126
61. Mangeol, P., Prevo, B., and Peterman, E. J. (2016) KymographClear and KymographDirect: two tools for the automated quantitative analysis of molecular and cellular dynamics using kymographs. *Mol. Biol. Cell* **27**, 1948–1957